The Astrophysical Journal, 600:96–105, 2004 January 1

THE ORIGIN OF EMISSION AND ABSORPTION FEATURES IN TON S180 *CHANDRA* OBSERVATIONS

A. Różańska and B. Czerny
Nicolaus Copernicus Astronomical Center, Bartycka 18, PL-00-716 Warsaw, Poland; agata@camk.edu.pl, bcz@camk.edu.pl

A. Siemiginowska
Harvard Smithsonian Center for Astrophysics, 60 Garden Street, Cambridge, MA 02138; aneta@head-cfa.harvard.edu

and

A.-M. Dumont and T. Kawaguchi
Observatoire de Paris, Section de Meudon, Place Jules Janssen, F-92195 Meudon Cedex, France; anne-marie.dumont@obspm.fr, toshihiro.kawaguchi@obspm.fr
Received 2003 March 5; accepted 2003 September 5

ABSTRACT

We present a new interpretation of the Ton S180 spectrum obtained by the *Chandra* Spectrometer (Low Energy Transmission Grating). Several narrow absorption lines and a few emission disk lines have been successfully fitted to the data. We have not found any significant edges accompanying line emission. We propose an interpretation of narrow lines consistent with that of the recent paper by Krolik, in which a warm absorber is strongly inhomogeneous. Such a situation is possible in the so-called multiphase medium, where regions with different ionization states, densities, and temperatures may coexist in thermal equilibrium under constant pressure. We illustrate this scenario with theoretical spectra of radiation transferred through a stratified cloud with constant pressure (instead of constant density) computed by the TITAN code in plane-parallel approximation. Detected spectral features are faint, and their presence does not alter the broadband continuum. We model the broadband continuum of Ton S180 assuming an irradiated accretion disk with a dissipative warm skin. The set of parameters appropriate for the data cannot be determined uniquely, but models with low values of the black hole mass have too hot and radially extended a warm skin to explain the formation of soft X-ray disk lines seen in the data.

Subject headings: galaxies: active — galaxies: individual (Ton S180) — galaxies: nuclei — galaxies: Seyfert — X-rays: galaxies

1. INTRODUCTION

Narrow-line Seyfert 1 (NLS1) galaxies (Osterbrock & Pogge 1985) form a special class of active galactic nuclei (AGNs). Narrowness of the optical lines frequently correlates with the steepness of the soft X-ray spectra (Boller, Brandt, & Fink 1996), hinting for a connection of this class with soft-state Galactic sources. The overall spectra are sometimes well described by a disk emission superimposed on a broad IR–X-ray power-law component (Puchnarewicz et al. 2001), but in most cases the soft X-ray slope seems to be too shallow for an extension of a disk blackbody emission. Such a steep soft X-ray spectrum of a roughly power-law shape may form either as a result of Comptonization (e.g., Czerny & Elvis 1987) by a moderately hot material (in comparison with the very hot plasma responsible for the hard X-ray component in normal Seyfert 1 galaxies) or as a result of reflection by a strongly ionized material (e.g., Czerny & Życki 1994; Czerny & Dumont 1998). The established presence of a warm absorber seen in many of those objects (Collinge et al. 2001; Kaastra et al. 2002; Kaspi et al. 2002; Kinkhabwala et al. 2002; Leighly et al. 2002; Yaqoob et al. 2003) complicates the analysis. However, with the extremely good spectral resolution of *Chandra* and *XMM* the issue may be addressed through the careful analysis of the existing spectral features.

Ton S180 ($z = 0.06198$, corresponding to 286 Mpc for Hubble constant 65 km s^{-1} Mpc^{-1}) is an extreme case of an NLS1 galaxy with a low value of the FWHM of the Hβ line ($\sim$900 km s^{-1}; Wisotzki et al. 1995) and steep soft X-ray spectrum of photon index $\Gamma = 2.68$ (Comastri et al. 1998). The Galactic absorption toward the object is low ($N_{\rm H} = 1.52 \times 10^{20}$ cm^{-2}; Stark et al. 1992). The source was extensively observed in all energy bands. The broadband spectral energy distribution (SED) determined by Turner et al. (2002) indicates that most of the energy is emitted in the 10–100 eV band. Furthermore, *HST* data show typical emission lines as expected for a Seyfert 1 galaxy and the lack of absorption features. High-resolution spectra obtained by the *Far Ultraviolet Spectroscopic Explorer* (*FUSE*) reveal UV absorption by O VI and the absence of neutral hydrogen absorption, indicating a high ionization state for the absorbing gas.

High-resolution X-ray spectra of this object were recently obtained with the *XMM-Newton* and *Chandra* satellites. The *XMM-Newton* spectrum was steep and featureless (Boller et al. 2003). *Chandra* data also appeared predominantly featureless and are well represented by a single power law with some soft excess (Turner et al. 2001, 2002). The shape of the soft excess was fitted by a DISKBB model; however, plotted residua hinted for the possible presence of sharp spectral features (Fig. 1 of Turner et al. 2001).

Therefore, in the present paper we reanalyze *Chandra* data in some detail (§§ 2 and 3), using a new response matrix acisleg1D1999-07-22rmfN0002.fits and including any effects related to the contamination layer on ACIS-S. We note that the observation of Ton S180 was performed on day 143 of the *Chandra* mission when the effects of the contaminant were much smaller than currently observed. We detected several weak narrow absorption lines due to the material located at the

line of sight to the source. In addition, several individual disk lines are fitted with equivalent widths (EWs) in rough agreement with the predictions of the model of the illuminated accretion disk spectrum presented by Różańska et al. (2002, 2003).

In § 3.2.1 we discuss existing models (Kaastra et al. 2002; Kinkhabwala et al. 2002; and others) for fitting absorption by warm, partially ionized gas present in many AGNs. We point out, following Krolik (2002), that the warm absorber may not be the slab of constant density matter, but it is rather the distribution of regions with different densities and temperatures. Such a multiphase mixture of gas can exist under constant pressure, as a result of thermal instabilities (Krolik, McKee, & Tarter 1981).

Until now, the multiphase models of the warm absorber were not constructed because popular photoionization codes (XSTAR, CLOUDY) compute radiative transfer through the constant density matter. In § 4 we present a new set of models computed by the code TITAN (Dumont, Abrassart, & Collin 2000), which solves radiative transfer through the matter in a non-LTE approach. Introducing the assumption of constant pressure (not density) of the warm absorber, we obtain spectra with many absorption lines from the gas with strong temperature and density gradient. Our code is suitable for any optical thickness of the absorber; nevertheless, we consider regions with total column density of order of 10^{23} cm^{-2}, as suggested by Krolik (2002) to be a typical property of the warm absorber.

In § 5 we construct two global disk corona models trying to predict the slope of the observed continuum. The model with higher black hole mass ($M = 10^8\ M_\odot$) is more promising in the sense that emission lines from the disk are expected in the spectra, since hot skin does not cover the disk completely.

Section 6 is devoted to the discussion, while conclusions are listed in § 7.

2. *CHANDRA* OBSERVATIONS AND DATA REDUCTION

Ton S180 was observed with the *Chandra* satellite on 1999 December 14 for about 80 ks in ACIS-S/LETG configuration, as described by Turner et al. (2001, 2002). The resolution of LETG corresponds to an FWHM $\approx 1200 E_{\rm keV}$ km s^{-1} for the range of energies from 0.1 up to 6 keV. The source luminosity at this epoch (2–10 keV unabsorbed flux equal to 4.6×10^{-12} ergs s^{-1} cm^{-2} and 0.3–10 keV unabsorbed flux equal to 2.2×10^{-11} ergs s^{-1} cm^{-2}) was comparable to that during the *BeppoSAX* observation (2–10 keV: 4.2×10^{-12} ergs s^{-1} cm^{-2}; Comastri et al. 1998) and *XMM-Newton* observation (0.3–10 keV: 2.2×10^{-11} ergs s^{-1} cm^{-2}; Boller et al. 2003) and somewhat fainter than during the 12 days of *ASCA* monitoring (2–10 keV: 6.5×10^{-12} ergs s^{-1} cm^{-2}; Romano et al. 2002).

We obtained the data from the *Chandra* archive. The data were processed with the standard *Chandra* X-Ray Center (CXC) data processing pipeline ASCDS version 6.7.0. We analyzed the data using CIAO version 2.2 and follow the Grating Analysis Thread (CXC Web site) to extract the spectrum and create appropriate effective area files (ARF files). We combined both sides of the first-order spectrum. We used calibration database CALDB version 2.14; in particular, we applied acisD1997-04-17qeN0003.fits quantum efficiency file and acisleg1D1999-07-22rmfN0002.fits as response matrix. This formally allows us to study the entire energy range between 0.12 and 12.2 keV, although calibration uncertainties are higher below 0.3 keV, while the effective area drops significantly above $\sim$4 keV. After removing bad pixels and rebinning the data to achieve at least 20 counts per channel, we examined the energy between 0.18 and 6 keV. All spectral fits have been performed with the XSPEC 9.0 fitting package.

Since the beginning of the *Chandra* mission the ACIS-S detector has been accumulating a layer of a contaminant that affects any measurements at low energies (below $\sim$0.8 keV). Detailed effects of the contaminant are still being investigated by the CXC,[1] however, it is clear that the overall degradation of ACIS quantum efficiency and the presence of additional absorption features are time dependent. Ton S180 was observed on day 143 of the *Chandra* mission, and based on the currently available calibration data we expect that the instrument shows a maximum of $\sim$40%–15% degradation within the 0.28–0.6 keV range (i.e., maximum $\sim$40% in 0.28 keV and $\sim$15% in 0.6 keV). In the following we identify the possible absorption features due to the absorber in Ton S180 using the entire available energy range. We note here that some of the features at energies close to the edges of the contaminant (C, N, O, F K edge) may be affected. We use the available model, ACISABS, to include the contamination effects in the analysis.

3. SPECTRAL ANALYSIS

3.1. *Continuum*

In the first step, we fit the $N_{\rm H}$ value of Galactic absorption together with a broken power law continuum. Our best-fit value of $N_{\rm H(Gal)} = (1.83 \pm 0.15) \times 10^{20}$ cm^{-2} is slightly larger than Galactic absorption $N_{\rm H(Gal)} = (1.5 \pm 0.5) \times 10^{20}$ cm^{-2}, determined by Dickey & Lockman (1990) and used by Comastri et al. (1998), or than $N_{\rm H(Gal)} = 1.52 \times 10^{20}$ cm^{-2}, determined by Stark et al. (1992) and used by Turner, George, & Nandra (1998) and Turner et al. (2001). All fitted parameters for "plain continuum" are listed in Table 1.

In the next step we fit a broken power law with the value of Galactic absorption fixed at $N_{\rm H(Gal)} = 1.52 \times 10^{20}$ cm^{-2} (see Table 1, second row). It results in slightly higher χ^2, but the power-law index below 2 keV is $\Gamma_1 = 2.69 \pm 0.02$ and agrees with the best-fit slope $\Gamma = 2.68$ presented by Comastri et al. (1998) for *BeppoSAX* data. The lower value obtained by Turner et al. (2001, 2002), equal to 2.44 ± 0.04, resulted from the use of an additional component to model the soft X-ray excess.

The energy break obtained by us in both models (about 1.7 ± 0.14 keV) is somewhat lower than the value determined by Comastri et al. (1998; $E_{\rm break} = 2.5$), but the spectral slope above this energy break, $\Gamma_2 = 2.26 \pm 0.07$, agrees with the results of Comastri et al. (1998).

Since both broken power-law indices are very similar to those obtained from other satellites, we adopt the second model (fixed Galactic absorption) for further analysis, leaving $\chi^2 = 1197$ per 1682 degrees of freedom (dof; reduced $\chi^2 = 0.7105$).

After fitting the continuum, there is still some structure in the residuals of the soft X-ray spectrum, suggesting the presence of absorbing matter along the line of sight toward the source. Therefore, we have tried to determine the column density of this gas in the simplest way, by fitting O VII, O VIII, and C VI edges often seen in Seyfert galaxies (Mrk 509,

[1] See http://asc.harvard.edu/cal/Acis/Cal_prods/qeDeg/index.html.

TABLE 1
LETG Continuum Fit in the 0.1–6.0 keV Energy Range

Model	$N_{H(Gal)}$ (10^{20} cm^{-2})	Γ_1	E_{break} (keV)	Γ_2	χ^2/dof
Plain continuum.....	$1.8277^{+0.152}_{-0.149}$	$2.755^{+0.038}_{-0.0367}$	$1.659^{+0.153}_{-0.109}$	$2.265^{+0.062}_{-0.065}$	1185/1681
Fixed $N_{H(Gal)}$	1.52	$2.689^{+0.022}_{-0.019}$	$1.771^{+0.134}_{-0.169}$	$2.261^{+0.074}_{-0.070}$	1197/1682
With lines.....	$1.527^{+0.1512}_{-0.14}$	$2.682^{+0.039}_{-0.0359}$	$1.604^{+0.12}_{-0.147}$	$2.295^{+0.0549}_{-0.0564}$	932/1624

Yaqoob et al. 2003; NGC 3783, Kaspi et al. 2002). Surprisingly, such edges appeared to be very weak in the data of Ton S180. We were able only to give upper limits for $\tau_{O\ VII}$, $\tau_{O\ VIII}$, and $\tau_{C\ VI}$ of order of 10^{-4}, which practically indicates the lack of those edges.

3.2. *Spectral Features*

3.2.1. *Application of Standard Warm Absorber*

X-ray absorption lines appear to be a common feature in many AGNs. The widely acceptable explanation is the existence of warm, ionized gas that is illuminated by the energetic radiation from the nucleus. In trying to find properties of the warm absorber, we need proper tools to fit those data. Until now, models of absorption by the partially ionized plasma available in XSPEC (ABSORI, PHOTO) assumed a slab with constant density.

In ABSORI, the radiative transfer of lines is not computed at all; only photoionization cross sections are determined and absorption "on the spot" is computed, $F_{out} = F_{in} \exp(-\tau_{line})$ (Done et al. 1992). Constructed by Kinkhabwala et al. (2002), the local PHOTO model[2] neglects photoelectric absorption but allows for individual line absorption, treating each ionic column density separately with an initially unabsorbed power law. This method produces consistent results only when absorbing matter is optically thin and transmitted spectra do not display photoelectric edges. Furthermore, they have assumed that plasma is optically thin to reemitted photons.

With the aim of finding evidence for a warm absorber in Ton S180, we have applied ABSORI to our data. Allowing for three parameters to be fitted in this model, χ^2 decreases by 38 (now reduced $\chi^2 = 0.747$). The fit indicates that the medium has column density $(7.34^{+0.23}_{-0.22}) \times 10^{21}$ cm^{-2} and ionization parameter $\xi = 4178^{+2082}_{-1328}$ for the fixed default temperature $T_{abs} = 3 \times 10^4$ K. This model, however, leaves considerable residual trends and does not allow for a deeper insight into the ionization state of the absorbing material. It is not surprising, since the model is based on simple computations of photoionization cross sections without accurate transfer through the medium.

We have applied PHOTO to our analysis. The model again indicates very low column densities of each ion, about 10^{14} cm^{-2} for C VI, O VII, and O VIII. We conclude that most probably the warm absorber in Ton S180 is more complicated than the optically thin constant density slab. It may be the stratified density gas, where accurate radiative transfer, including all photoionization processes, should be calculated to model the transmitted spectrum. Such models are not available for fitting the data yet, so two or three separate absorbers with different constant densities and ionization states are used together to explain spectral features in some AGNs (Kaastra et al. 2002; Kaspi et al. 2002). This motivates us to present in § 4 the model of the multiphase gas with stratified density and temperature, where the radiative transfer of incident power law is carefully computed. The model is not ready for fitting yet but gives interesting results based on EWs of various lines. Observed line properties in the Ton S180 data are determined in the section below.

More advanced modeling was done with the code XSTAR (developed by Kallman & Bautista 2001), which allows us to estimate the total column densities of absorbed gas. Models are computed assuming a constant density slab. Such models are very useful for reconstruction of the flat part of the curve of growth (Yaqoob et al. 2003) and for subsequent estimation of turbulent velocities of the absorber. Nevertheless, at the last stage of analysis separate Gaussian components are fitted to the data.

3.2.2. *Absorption Lines*

We have successfully fitted several absorption lines using a standard Gaussian model for each line separately (see Figs. 1–7. The Gaussian fit requires three free parameters: energy of the line centroid, Gaussian width, and normalizations, which has to be negative in the case of absorption lines. We include in the fit only those features that are significant. All absorption lines are presented in Table 2. For each line we list its central energy in keV, EW in eV, the decrease of χ^2, and the best identification with observed and rest-frame energy and with possible blends.

Some of those lines, especially the softest ones, may be caused by dust presented on *Chandra* mirrors. This should show up as a common feature in all objects, even those with different redshifts. To check whether lines are real or instrumental, we compare observations of Ton S180 with *Chandra* data of quasar 3C 273 observed 2 weeks later with the same configuration as Ton S180. Exemplary residuals (for soft range 0.2–0.24 keV) for both objects are shown in Figure 8. In both cases the local power law was fitted with a fixed value of Galactic absorption appropriate for each object. The same features around energy 0.22 keV are present as well in 3C 273 with redshift 0.156 as in Ton S180. We repeated such an analysis in the whole energy range. All possible instrumental lines are labeled in Table 2.

Some of the detected features are seen only in the Ton S180 spectrum and therefore seem to be real, intrinsic to the source. For example, in Figure 9 we show that line C VI with observed energy 0.4428 keV, which is detected in Ton S180 data, is not seen in 3C 273.

Lines are very faint. They usually have EW less than or about 2 eV, and several of them are just marginal detections, as clearly seen from the line EW error, given at 90% confidence level (each error is computed for the one parameter of interest). Only two of them are stronger, but from theoretical

[2] See http://xmm.astro.columbia.edu/research.html.

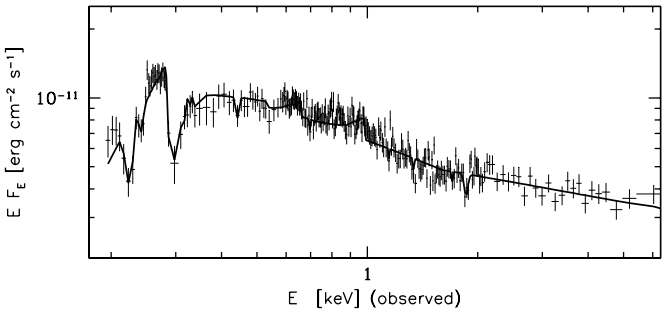

FIG. 1.—LETG spectrum of Ton S180. The solid line denotes the total model after the broken power law, Galactic absorption, and all lines have been fitted.

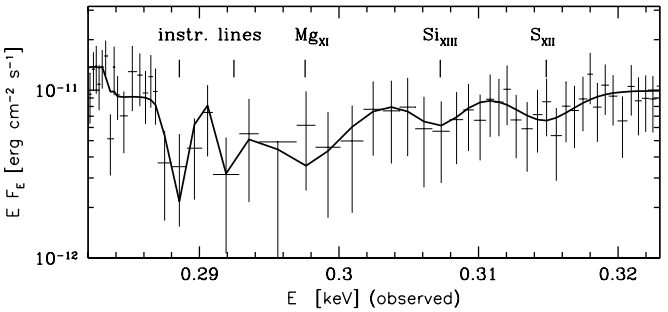

FIG. 3.—Same as Fig. 2, but for 0.282–0.32 keV

predictions by analyzing our modeled spectra from § 4, they are not blends. All possible blends according to our modeled spectra obtained with spectral resolution 100 are listed in Table 2. There is therefore no major discrepancy between the *Chandra* results and the *XMM* observations (Boller et al. 2003) where only upper limits of order of 1 eV at energies 0.35–0.7 keV were provided. Most lines originate from hydrogen- or helium-like ions, indicating that matter is highly ionized. There is an absence of lines from mildly ionized species.

Interestingly, we found two different transitions from the same element at the given ionization level [C VI$_{(1-2)}$ and C VI$_{(1-5)}$, where i–j denotes the number of levels from and to which the transition proceeds]. This is helpful in the aim to estimate the optical thickness of C VI ions and then total optical thickness of the warm absorber.

If the medium is optically thin in those lines (i.e., weak-line case), we are on the linear part of the curve of growth, where EW is proportional to the column density N_i of the absorbed ion:

$$\mathrm{EW}_\nu = \frac{\pi e^2}{m_e c} N_i f_{ij}, \tag{1}$$

where f_{ij} is the oscillator strength transition and stimulated emission has been set equal to unity. Thus, for the given population of ions at the same ionization level, the ratio of EWs is given by

$$\frac{\mathrm{EW}_{ij}}{\mathrm{EW}_{ik}} = \frac{f_{ij}}{f_{ik}}. \tag{2}$$

Since the oscillator strengths are strictly atomic features independent from the radiation field and are calculated theoretically, we use them to find the ratio

$$\frac{\mathrm{EW}\left[\mathrm{C\ VI}_{(1-2)}\right]}{\mathrm{EW}\left[\mathrm{C\ VI}_{(1-5)}\right]} = 29.86. \tag{3}$$

On the other hand, the same ratio determined for Ton S180 (see Table 2) equals $0.62^{+3.53}_{-0.59}$. Error is computed assuming the most pessimistic case, when the numerator has its maximal value EW + ΔEW and the denominator has its minimal value EW − ΔEW. Although the error is huge, the value of the ratio determined from observation is still far from theoretical predictions for the optically thin medium (eq. [3]). Our theoretical spectra (see § 4) suggest that the C$_{(1-2)}$ line is possibly a blend with Mg XII, Si XIV, and most strongly with C V. We have computed that the real EW of the C$_{(1-2)}$ line can be even up to 4 times lower than the EW of the whole blend. However, this fact even lowers the observed ratio of EWs of two carbon lines.

The straight conclusion is that the emitting region is optically thick for those lines and the transfer in lines should be taken into account for proper modeling of the warm absorber. It is also possible that the identification of the lines is not correct or the line is a blend of the carbon line with another transition. Nevertheless, we further explore the possibility that the carbon line ratio is determined correctly.

Therefore, equation (1) gives only a lower limit for the ion column density, equal to 3.6×10^{16} cm^{-2} from the C VI$_{(1-2)}$ line and 1.7×10^{18} cm^{-2} from C VI$_{(1-5)}$, which under the assumption that all carbon is in the form of C VI ions and with solar abundances translates into the lower limit for the warm absorber column equal to 1.1×10^{20} and 5.1×10^{21} cm^{-2}, respectively.

Exact determination of the column density is complicated. At the flat curve of growth we need additional information

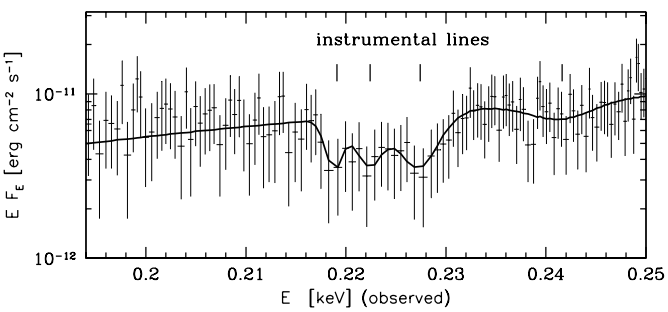

FIG. 2.—Observed spectrum with the best-fit model for 0.19–0.25 keV

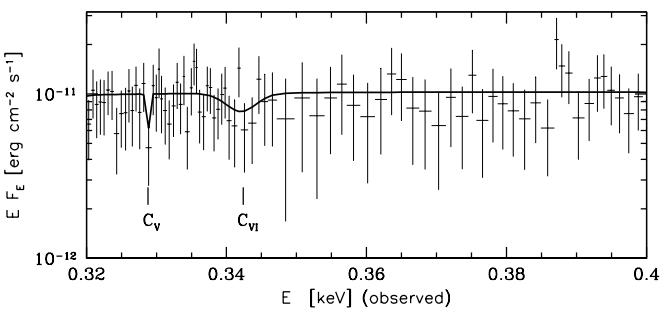

FIG. 4.—Same as Fig. 2, but for 0.32–0.4 keV

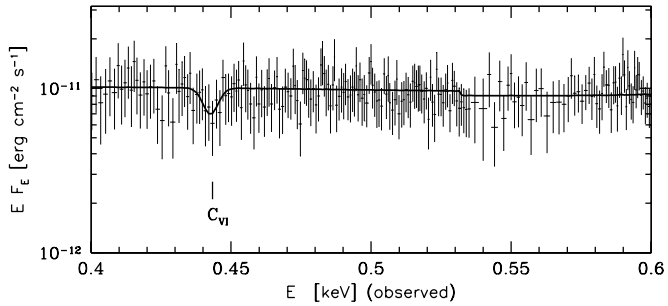

FIG. 5.—Same as Fig. 2, but for 0.4–0.6 keV

about velocity dispersion b to indicate column densities. In the case of considered data this is very difficult because the 1 σ error of FWHM is too high to estimate the b parameter. For instance, for the S XII line, presented in Figure 3, FWHM $= (5^{+16}_{-1}) \times 10^3$ km s^{-1}. This fact also precludes us to integrate over the fitted line profile in the aim of determining the exact flux emitted in this line. Thus, we are unable to compute the exact optical depth of the line and therefore the column density of the absorbing ion. The number of lines is too small to fit the full model (for instance, XSTAR).

Another lower limit on column density of the C VI ion can be derived knowing that the optical thickness of the C VI lines is higher than 1. In such a case we can write

$$N_i > \frac{m_e c}{\pi e^2 f_{ij}} \mathrm{FWHM} = \frac{1.665 m_e \nu_0}{\pi e^2 f_{ij}} \sqrt{\frac{2kT}{A_i m_{\mathrm{H}}}}, \quad (4)$$

where T is the temperature of the medium and A_i is atomic mass of the ion. For the C VI$_{(1-5)}$ line we obtain

$$N_{\mathrm{C\ VI}} > 6.33 \times 10^{13} \sqrt{T}. \quad (5)$$

For the temperature approximately equal to 10^6 K this value is 2 times higher than the one determined by Mason et al. (2003) in the case of Mrk 766. This limit is over an order of magnitude weaker than the limit obtained directly from equation (1). FWHM estimated from $T \sim 10^6$ K is quite narrow, and the line width is rather determined by much larger turbulent motion.

The value of reduced χ^2 was equal to 0.6363 after fitting all possible absorption lines.

3.2.3. *Disk Emission Lines*

After absorption lines have been identified, we were able to fit a few emission lines from an accretion disk. We applied the standard DISKLINE model with a fixed power-law index in the radial dependence of the irradiating flux $\beta = 2.7$. We assumed $r_{\mathrm{in}} = 6R_g$ and $r_{\mathrm{out}} = 1000R_g$ (where $R_g = GM/c^2$). We have found the best value of inclination angle $i = 30^\circ$ for the C V line, and we adopted it (keeping frozen) for the other lines. Results are listed in Table 3 and shown in Figures 1 and 10.

The last column of Table 3 presents theoretical values of EWs of the same emission lines computed for an accretion disk illuminated by hard X-ray flux equal to the local disk flux (full model presented in Różańska et al. 2002, 2003). The model takes into account harder incident radiation ($\Gamma = 1.9$) than is seen in the case of Ton S180 and solar metal abundances. For moderate illumination in the model we have found, for instance, the EW of Ne X equal to 11 eV, O VIII equal to 18.2 eV, Mg XII equal to 10.5 eV, and Fe XVII equal to about 8 eV, or many others at the same order of magnitude with respect to the reflected continuum (factor of 2–3 smaller with respect to the total continuum). Models do not predict lines with EWs higher than $\sim$20 eV, when the disk is in hydrostatic equilibrium (Różańska et al. 2002, 2003; see also figures in Nayakshin, Kazanas, & Kallman 2000; Ballantyne, Ross, & Fabian 2001). Higher values can only be obtained from the constant density medium, as discussed by Ballantyne, Ross, & Fabian (2002), particularly when adopting enhanced metallicity. Emission lines also become by a factor of a few stronger when the dynamical flare model is adopted; i.e., the timescale of the flare is shorter than the timescale for a disk surface layer to achieve hydrostatic equilibrium (Collin et al. 2003). However, in that case lines should be narrow and not represented well by a DISKLINE shape.

Soft disk line detection is therefore a promising tool to constrain the conditions within the cold reprocessing medium. Detection of standard broad disk lines presented in this paper, if real, suggests no strong departure from hydrostatic equilibrium and the extension of the cold disk roughly down to the marginally stable orbit.

After all lines have been fitted, we fit again a broken power law with Galactic absorption. Results presented in Table 1 (last row) indicate that lines do not affect continuum very strongly. The final value of reduced χ^2 appeared to be 0.5531.

4. PROPOSED MODEL OF THE WARM ABSORBER

In this section we present models of the warm absorber, allowing density, temperature, and consequently ionization state to be stratified (Krolik 2002). The only assumption that we made is the constant pressure. Such an approach is more realistic than the constant density model, since thermal instabilities can produce gas with steep ionization structure, keeping all zones in pressure equilibrium.

We have used the TITAN code (Dumont et al. 2000) to compute temperature and density structure of the warm

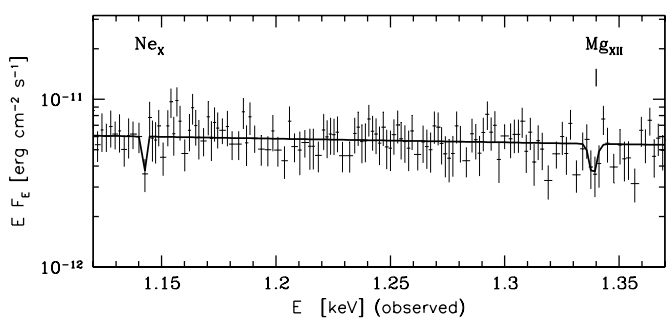

FIG. 6.—Same as Fig. 2, but for 1.12–1.37 keV

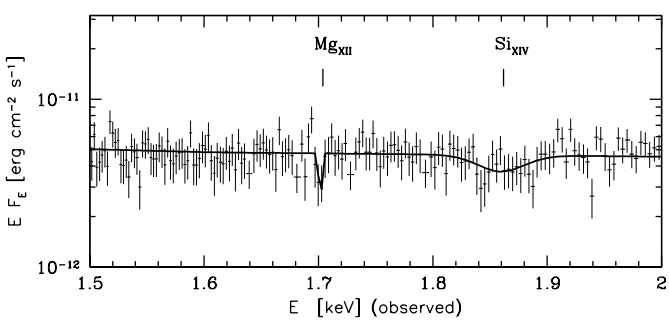

FIG. 7.—Same as Fig. 2, but for 1.5–2 keV

TABLE 2
ABSORPTION LINES FITTED TO THE *Chandra* DATA OF TON S180

Observed Energy (keV)	EW (eV)	$\Delta\chi^2$	Best Identification[a]
$0.2188^{+0.005}_{-0.014}$	1.39 ± 0.87	7.42	Instrumental
$0.2222^{+0.0011}_{-0.0010}$	2.05 ± 1.38	6.6	Instrumental
$0.2272^{+0.0008}_{-0.0009}$	3.62 ± 1.29	22.29	Instrumental
$0.2414^{+0.0028}_{-0.0036}$	1.87 ± 1.08	6.34	Instrumental
$0.2884^{+0.0007}_{-0.0006}$	1.82 ± 0.83	15.35	Instrumental
$0.2923^{+0.0012}_{-0.0012}$	1.39 ± 1.17	6.92	Instrumental
$0.2974^{+0.0018}_{-0.0022}$	6.31 ± 3.70	14.0	Mg XI (0.2971; 0.3155)
$0.3071^{+0.0026}_{-0.0030}$	2.26 ± 1.95	5.18	Si XIII (0.30878; 0.3279)
$0.3147^{+0.018}_{-0.030}$	2.05 ± 1.28	7.55	S XII (0.31899; 0.3387)
$0.3285^{+0.0009}_{-0.0006}$	0.39 ± 0.50	3.47	C V (0.33386; 0.3545)
$0.3421^{+0.0037}_{-0.0045}$	1.38 ± 1.30	4.45	C VI (0.3459; 0.3673) blend with Mg XII (0.368), Si XIV (0.3703), C V (0.3709)
$0.4426^{+0.024}_{-0.024}$	2.22 ± 1.58	5.16	C VI (0.4428; 0.4702)
$0.6963^{+0.015}_{-0.032}$	0.74 ± 0.69	3.47	Fe XVII (0.6868; 0.72932) blend with S XVI (0.731)
$1.142^{+0.0034}_{-0.0095}$	0.992 ± 1.18	3.29	Ne X (1.1387; 1.209) blend with Fe XXV (1.206), Fe XXV (1.208), and Fe XXV (1.213)
$1.339^{+0.0030}_{-0.0024}$	1.48 ± 1.84	2.95	Mg XII (1.3861; 1.472)
$1.702^{+0.030}_{-0.032}$	1.88 ± 2.38	3.7	Mg XII (1.7327; 1.840) blend with Si XIII (1.853)
$1.860^{+0.013}_{-0.016}$	10.6 ± 5.24	6.09	Si XIV (1.8831; 2.000)

[a] Expected observed energy and the rest-frame energy in keV for identified lines are given in parentheses; for blends only rest-frame energy is listed.

absorber together with radiative transfer. The code is based on two-stream approximation and works in plane-parallel geometry. Radiative transfer is computed both in lines and in continuum so the code can be used for very inhomogeneous or even optically thick media. Thermal, ionization, and statistical equilibrium of ions are computed in complete non-LTE for 10 elements and all corresponding ions. We consider the following elemental abundances: H: 1; He: 0.085; C: 3.3×10^{-4}; N : 9.1×10^{-5}; O: 6.6×10^{-4}; Ne: 8.3×10^{-5}; Mg: 2.6×10^{-5}; Si: 3.3×10^{-5}; S: 1.6×10^{-5}; Fe: 3.2×10^{-5}. We transfer a total of 721 lines of different ions, taking their oscillator strengths and energies from the National Institute of Standards and Technology[3] (NIST). Photoelectric absorption is fully taken into account.

In our models, we have assumed the shape of incident radiation consistent with this fitted to the data of Ton S180. We have adopted the power-law photon index $\Gamma = 2.6$ (§ 3.1) and spectral limits from 0.012 up to 100 keV as we have concluded from the broadband SED presented by Turner et al. (2002).

The assumption of constant pressure refers to the total radiation and gas pressure, and its value is self-consistently determined by the code. The ionization parameter on the top of the absorber ξ_0 and the total column density are free parameters of our models. We have computed models for $\xi_0 = 10^5$ and $N_{\rm tot} = 1.7 \times 10^{23}$ cm^{-2} named A1, $\xi_0 = 1000$ and $N_{\rm tot} = 6.8 \times 10^{22}$ cm^{-2} named A2, and $\xi_0 = 10^7$ and $N_{\rm tot} = 1.7 \times 10^{23}$ cm^{-2} named A3. Such values of column densities for given ξ_0 are upper limits above which the optical depth of the cloud is large enough that strong absorption edges become present in outgoing spectra.

Even for high ξ_0, the maximum Compton temperature is low, $T_{\rm Compt} = 2.1 \times 10^6$ K, because the incident spectrum is soft ($\Gamma = 2.6$).

[3] See http://physics.nist.gov.

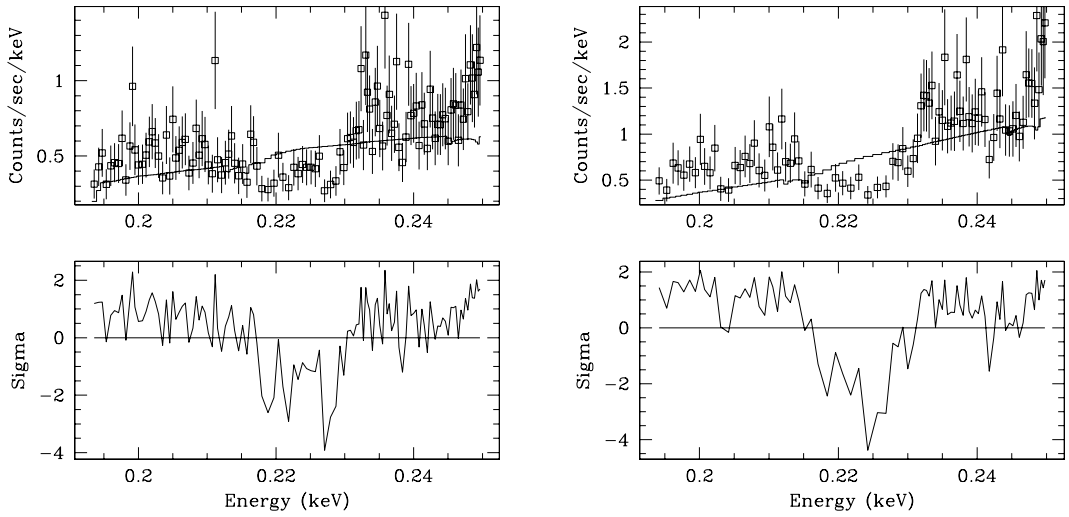

FIG. 8.—Comparison of *Chandra* data of Ton S180 to the *Chandra* data of 3C 273 for energies between 0.20 and 0.24 keV. Similar structure in residuals around 0.22 keV is present in both objects.

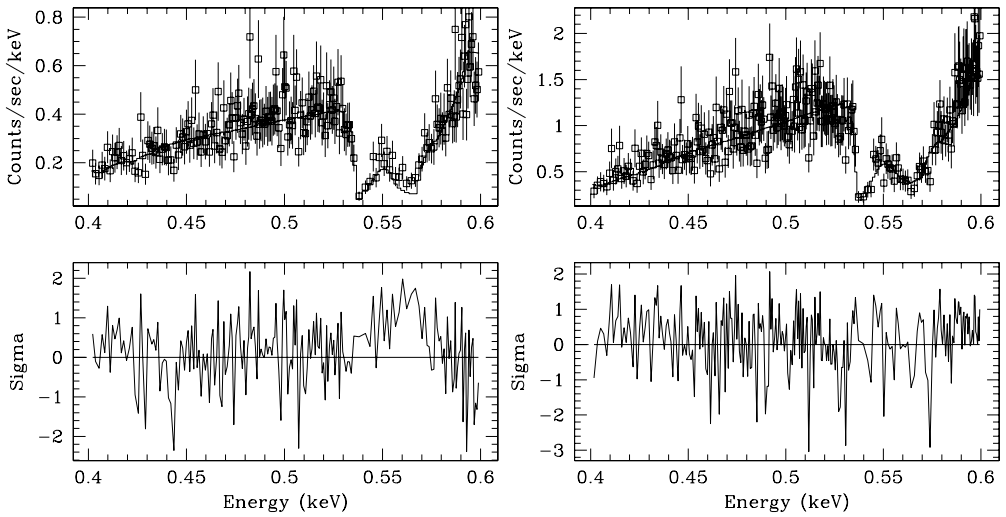

FIG. 9.—Comparison of *Chandra* data of Ton S180 to the *Chandra* data of 3C 273 for energies between 0.4 and 0.6 keV. The 2 σ structure presented in Ton S180 around 0.44 keV is clearly absent in 3C 273 data.

In Figure 11 we show the temperature structure for A1 (*dashed line*; higher ξ_0 does not change this structure) compared to A2 (*solid line*), and in Figure 12 we show the corresponding spectra. In the case of higher ξ_0 (model A1) the temperature range within the medium is much broader and the effective spectrum from such a region (presented in Fig. 12, *dashed line*) displays slightly stronger lines than for A2 (*solid line*). We have enlarged the range of frequencies to illustrate the region observed in Ton S180 data.

We have also performed a comparison of the A1 model to the warm absorber with constant density (Fig. 11, *dot-dashed line*) assuming that both clouds have the same total column densities and are illuminated by the equivalent fluxes. Thus, choosing the volume density for the constant density cloud, the ionization parameter is determined by the value of flux the same as for the stratified cloud. We have chosen volume density equal to 3×10^{13} cm^{-3}, which implies $\xi_0 = 300$. The spectrum for the constant density cloud presented in Figure 12 by the dot-dashed line displays strong edges and cannot explain our observations. Decreasing volume density, we increase ionization parameter, and it may remove edges. We plan to make proper calculations in future work to show how to distinguish between the low constant density cloud and the stratified cloud.

We have also calculated theoretical values of the EWs of transferred lines, the same that are found in Ton S180 data. Results are presented in Table 4. EWs for high surface ionization (A1) are almost a factor of 2 higher than for the A2 model. In our data we see slightly larger EWs and we cannot model them by increasing ξ_0, since model A3 shows the same EWs as A1.

Therefore, we have to introduce the model labeled A4 in Table 4, which has exactly the same parameters as A2, i.e., $\xi_0 = 1000$ and $N_{\rm tot} = 6.8 \times 10^{22}$ cm^{-2}, and we also assume a turbulent velocity $v_{\rm turb}/c = 3 \times 10^{-4}$. Turbulent velocity does not change the total temperature structure; it only affects lines, making their EWs higher, as shown in Table 4. For model A4 several lines (for instance, Mg XI, Si XIII, S XII, C VI, and Si XIV) have EWs in quite good agreement with those achieved from observations (see Table 2).

In all presented models the ratio of EW[C VI$_{(1-2)}$]/EW [C VI$_{(1-5)}$] equals 0.7, in very good agreement with the observed value of 0.6.

5. BROADBAND CONTINUUM

In order to draw attention to the possible constraints resulting from detection of the broad disk lines, we model the broadband spectrum of Ton S180 assuming three basic spectral components: (1) an illuminated accretion disk, (2) an optically thick Comptonizing plasma, and (3) an optically thin (nonthermal) Comptonizing plasma. For low or moderate accretion rate we take the simplest Keplerian disk model, emitting locally as a blackbody and parameterized fully by the black hole mass, M, and accretion rate, $\dot{m}$, given in Eddington units (taking efficiency 1/12 appropriate for the Newtonian model). We consider also the highly supercritical accretion disk applying the model described by Kawaguchi (2003). This model includes the effect of strong radial advection and the departure from the local blackbody emission due to electron scattering, which are essential at very high accretion rates.

We assume that the energy generated in the inner disk illuminates the outer disk, with the irradiating flux $\propto r^{-2-\beta}$,

TABLE 3
EMISSION DISK LINES FITTED TO THE *Chandra* DATA OF TON S180

Observed Energy (keV)	EW (eV)	$\Delta\chi^2$	Best Identification	EWs from Illuminated Disk[a]
$0.2704^{+0.002}_{-0.0007}$	15.3 ± 2.63	72.73	C V (0.2899; 0.3079)	8.69
$0.6300^{+0.014}_{-0.01}$	13.5 ± 4.89	21.26	O VIII (0.6149; 0.653)	19.0
$0.9403^{+0.007}_{-0.021}$	30.7 ± 7.41	46.26	Ne X (0.961; 1.020)	11.29

[a] Theoretical EWs are computed with respect to reflected continuum.

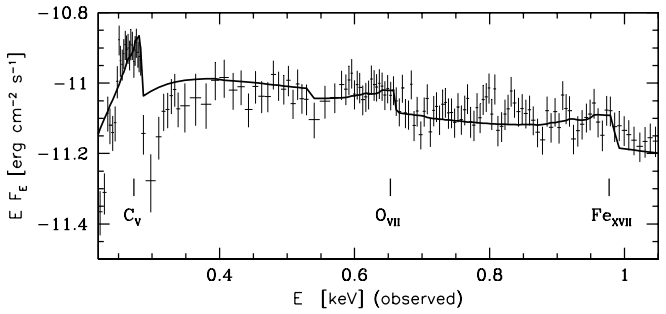

FIG. 10.—Same as Fig. 2, but for 0.22–1.05 keV. Three emission lines fitted to the spectrum of Ton S180 are seen.

with $\beta = 0.1$. This irradiation effect may come from the scattering of the disk radiation back toward the disk by the warm absorber, as well as from the direct interception of the radiation by the flaring outer disk. We adopted a simple parameterization and did not model this irradiation since the process is quite complex. It would require assumption about the radial and angular distribution of the density of the scattering medium (see, e.g., Kurpiewski, Kuraszkiewicz, & Czerny 1997) and the computations of the viscosity-dependent disk vertical structure, as in Różańska et al. (1999). We did not compute the disk vertical structure in order to verify whether the outer disk is flaring strongly enough to allow for such a strong effect.

We assume that the inner disk for $r < r_{\rm skin}$ is fully covered by the optically thick plasma. Thermal plasma parameters are the optical depth, τ, and the temperature, T. Only soft photons from the inner disk come through this plasma, and we compute the spectrum using the simple code based on the Sunyaev & Titarchuk (1980) description (used, for example, by Collin-Souffrin et al. 1996). We adopt the plane-parallel geometry and the generation of the photons at the bottom of the zone. This component forms a soft X-ray component of the spectrum. We next added a contribution from a much hotter, or nonthermal, plasma component in order to provide the appropriate hard X-ray tail, but the parameters of this component are poorly constrained and we do not address this issue in detail.

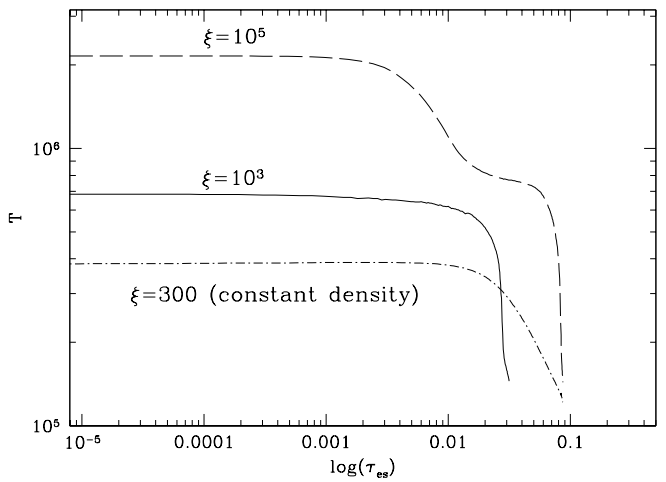

FIG. 11.—Temperature distribution for models with $\xi = 10^5$, $N_{\rm tot} = 1.7 \times 10^{23}$ cm^{-2} (*dashed line*) and $\xi = 10^3$, $N_{\rm tot} = 6.8 \times 10^{22}$ cm^{-2} (*solid line*). The constant density case for $\xi = 300$, $N_{\rm tot} = 1.7 \times 10^{23}$ cm^{-2} is presented by the dot-dashed line.

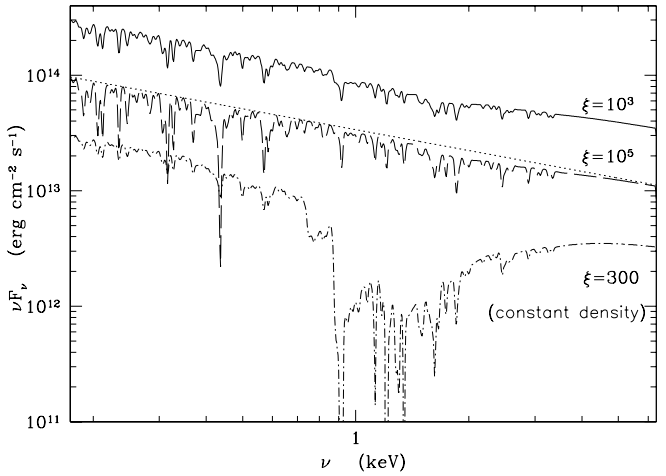

FIG. 12.—SED (spectral resolution 60) for models with $\xi = 10^5$, $N_{\rm tot} = 1.7 \times 10^{23}$ cm^{-2} (*dashed line*) and $\xi = 10^3$, $N_{\rm tot} = 6.8 \times 10^{22}$ cm^{-2} (*solid line*). The constant density case for $\xi = 300$, $N_{\rm tot} = 1.7 \times 10^{23}$ cm^{-2} is presented by the dot-dashed line. Both solid and dot-dashed lines are arbitrarily moved to see differences. The dotted line indicates the slope of the incident continuum.

Our model provides a one-parameter family of solutions for the broadband spectrum; i.e., we can find a good model for any mass of the black hole between 1×10^7 and $1 \times 10^8\ M_\odot$, but for a fixed mass all other parameters ($\dot{m}$, $r_{\rm skin}$, τ, and T) are uniquely determined. The appropriate accretion rate is needed to reproduce the normalization of the spectrum in the optical band, where it is mostly given by the product of $M^2\dot{m}$ (for the illumination case). The value of $r_{\rm skin}$ must be chosen in order not to overproduce/underproduce far-UV flux. The slope of the soft X-ray spectrum gives one constraint on the combination of τ and T, but for low values of T, which are always derived, the normalization of the soft Comptonized spectrum also depends significantly on the plasma parameters (for a number of soft photons already specified by $r_{\rm skin}$).

Examples of the solution are therefore as follows: for $M = 10^8\ M_\odot$ we have $\dot{m} = 0.07$, $r_{\rm skin} = 20R_g$, $\tau = 17$, $T = 0.65$ keV, and for the high accretion rate case $M = 10^7\ M_\odot$ we have $\dot{m} = 83$, $r_{\rm skin} = 140R_g$, $\tau = 2.5$, $T = 12$ keV; the broadband data fitted for the largest mass are shown in Figure 13 and for the smallest mass in Figure 14.

Those two extreme models differ considerably with the extension of the disk part covered with the hot skin. In the case of small mass, the disk model would overpredict the far-UV data points considerably if the large portion of the inner disk is not fully covered with the thermal plasma. Plasma parameters are such that they make formation of any emission lines rather difficult.

In the case of high mass the inner disk does not really have to be covered, as indicated by the much smaller value of $r_{\rm skin}$. The clumpy corona model would be easily applicable to this case, or even the X-ray emission could come from some shocks in outflowing material at the rotation axis. The fraction of the disk covered may be always further reduced assuming that synchrotron emission of the plasma itself provides additional soft photons. In such a case the lines from the irradiated disk are easily expected.

6. DISCUSSION

6.1. *Warm Absorber*

Reanalyzing *Chandra* data of NLS1 galaxy Ton S180, we were able to identify several narrow absorption lines due to

TABLE 4
EQUIVALENT WIDTH (eV) OF ABSORPTION LINES FOR SEVERAL MODELS COMPUTED BY TITAN

Ion	Transition	A1	A2	A3	A4
S VIII	$2s^2 2p^5\ ^2P^o$–$2s^2 2p^5 3d^2 L$	0.522	0.293	0.506	1.431
Fe XV	$3s^2\ ^1S$–$3s4p\ ^1P^o$	0.406	0.191	0.392	1.164
Si X	$2s^2 2p\ ^2P^o$–$2s^2 3d\ ^2D$	0.584	0.286	0.568	1.193
S X	$2s^2 2p^3\ ^4S^0$–$2s^2 2p^2(^3P)3l\ ^4P$	0.585	0.305	0.567	1.549
C V	$1s^2\ ^1S$–$2p\ ^1P^o$	1.112	0.587	1.079	1.849
S XI	$2s^2 2p^2\ ^3P$–$2s^2 2p 3d\ ^3L^o$	0.680	0.333	0.659	1.500
Mg XI	$2p\ ^3P^o$–$4l\ ^3L$	0.834	0.468	0.809	1.995
Si XIII	$2s\ ^1S$–$3p\ ^1P^o$	0.783	0.439	0.759	2.019
S XII	$2s^2 2p\ ^2P^o$–$2s^2 3d\ ^2D$	0.719	0.348	0.697	1.580
C V	$1s^2\ ^1S$–$3p\ ^1P^o$	1.287	0.708	1.249	2.151
C VI	$1s\ ^2S$–$2l\ ^2L$	1.186	0.599	1.136	1.772
C VI	$1s\ ^2S$–$5l\ ^2L$	1.650	0.881	1.585	2.585
Fe XVII	$2s^2 2p^6\ ^1S$–$2s^2 2p^5 3s\ ^1P^o$	1.216	0.621	1.159	4.008
Ne X	$1s\ ^2S$–$3l\ ^2L$	3.151	1.856	3.063	7.485
Mg XII	$1s\ ^2S$–$2l\ ^2L$	3.561	2.101	3.561	9.107
Mg XII	$1s\ ^2S$–$4l\ ^2L$	5.224	2.947	5.330	12.26
Si XIV	$1s\ ^2S$–$2l\ ^2L$	4.594	2.426	4.598	11.56

NOTE.—Here l means that the configuration is a mixture of multiplets spd.

the warm absorber. Such lines were neither discussed by Turner et al. (2001, 2002), who presented the data for the first time, nor seen in *XMM-Newton* data (Boller et al. 2003) because the lines are indeed very faint. We detected lines of highly ionized carbon and other elements, but we do not seem to detect any oxygen lines, while in the *FUSE* data (Turner et al. 2002) O VI narrow absorption line components were seen.

Five of those absorption lines detected in Ton S180 (C VI [$E = 0.3673$ keV], Ne X, Mg XII [$E = 1.471$ keV], Mg XII [$E = 1.840$ keV], and Si XIV) are also seen in another Seyfert 1 galaxy, NGC 3783, analyzed by Kaspi et al. (2002), with similar values of EWs (0.46, 2.3, 4.3, 1.6, and 6.6 eV, respectively). In addition, Kaastra et al. (2002) have found in NGC 5548 the same C V, C VI ($E = 0.3673$ keV), Ne X, Mg XII ($E = 1.471$ keV), and Si XIV, with the following EWs: 0.26, 0.99, 0.47, 3.09, and 3.88 eV, respectively.

We found a lower limit for the warm absorber column of 5.1×10^{21} cm^{-2} from the EW of one of the C VI lines (see § 3.2.2) and an upper limit of 1.7×10^{23} cm^{-2} from our model of the warm absorber (see § 4). The upper limit is not firm since it is sensitive to the adopted turbulent velocity, as well as abundances.

6.2. *Broadband Continuum*

The *Chandra* data show that the effect of the warm absorber does not modify significantly the X-ray spectrum in the case of

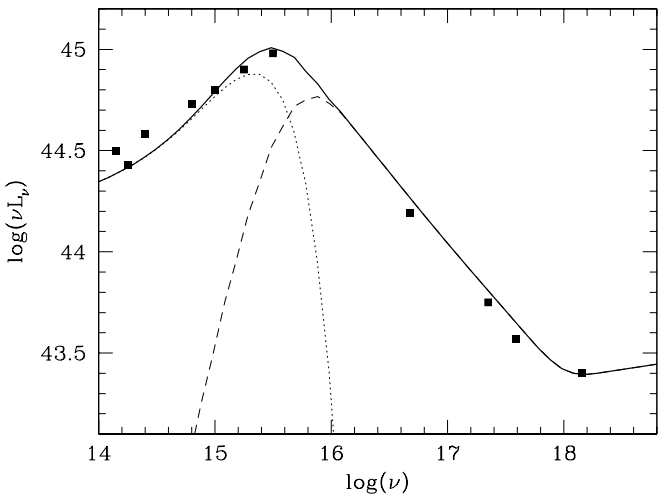

FIG. 13.—Model of the broadband spectrum of Ton S180 (*solid line*) for the minimum acceptable accretion rate. The dotted line gives the spectrum of the outer uncovered part of the disk, and the dashed line shows the radiation from the inner disk after passing through the Comptonizing medium. Model parameters: $M = 10^8\ M_\odot$, $\dot{m} = 0.07$, $r_{\rm skin} = 20R_g$, $\tau = 17$, $T = 0.65$ keV.

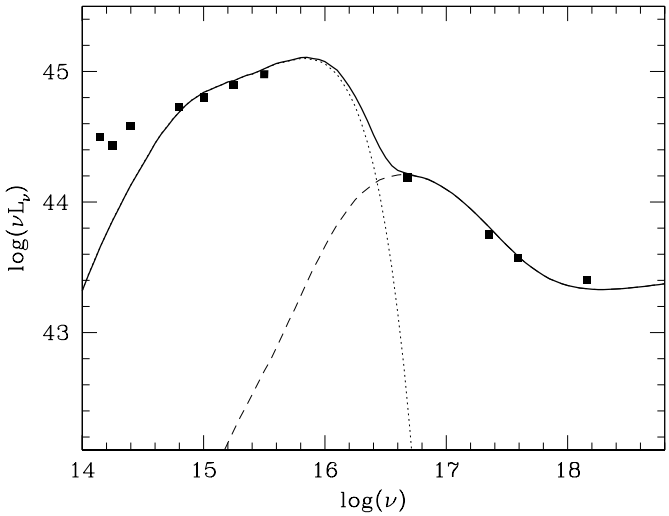

FIG. 14.—Model of the broadband spectrum of Ton S180 (*solid line*) for very high accretion rate (Kawaguchi 2003) . The dotted line gives the spectrum of the outer uncovered part of the disk, and the dashed line shows the radiation from the inner disk after passing through the Comptonizing medium. Model parameters: $M = 10^7\ M_\odot$, $\dot{m} = 83$, $r_{\rm skin} = 140R_g$, $\tau = 2.5$, $T = 12$ keV.

Ton S180. Therefore, our analyses do not change the overall picture of the Ton S180 continuum, as shown by Turner et al. (2002) and discussed by Boller et al. (2003). In particular, the huge soft X-ray excess is reasonably explained only within the frame of the Comptonization model.

Variability arguments presented by Boller et al. (2003) in favor of the hybrid plasma model (thermal plasma being responsible for the soft X-ray slope and nonthermal plasma component leading to hard X-ray power law) are convincing. However, the data do not allow us to determine all the hybrid plasma parameters uniquely, as explained by Boller et al. (2003), so in the present paper we have used a much simpler model in order to draw attention to the possible constraints resulting from detection of the broad disk lines.

Those emission lines can be present in the broadband spectrum rather for higher black hole mass $M = 10^8\ M_\odot$ and accretion rate $\dot{m} = 0.07$, since with those assumptions hot skin does not cover the disk completely. This conclusion differs from the black hole mass estimations done for Ton S180 by Wang & Lu (2001), who found $M = 1.3 \times 10^7\ M_\odot$. However, our result is consistent with studies done by A. Siemiginowska (1997, private communication), where a simple disk corona model was fitted to the *BeppoSAX* data (those presented by Comastri et al. 1998).

7. CONCLUSIONS

We argue, contrary to the previous papers by Turner et al. (2001) and Boller et al. (2003), that spectral features in absorption and even in emission are present in the *Chandra* data of Ton S180. The quality of the data does not allow us to determine column densities of individual metals; we can only put a lower limit on the column density of C VI.

The lack of edges in the spectrum gives an upper limit on total column density, which is 1.7×10^{23} cm^{-2} for the best computed model ($\xi_0 = 10^5$).

A few emission lines fitted to the Ton S180 *Chandra* data have lower EWs by a factor of 6 than those reported by Mason et al. (2003) for Seyfert 1 galaxy Mrk 766 but of similar order as disk lines found by Kaastra et al. (2002) in NGC 5548.

Estimation of the mass of the black hole in Ton S180 based on FWHM of the Hβ line and the formula of Kaspi et al. (2000) for the relation between the size of the broad-line region and the object luminosity at 5100 Å rather suggests small black hole mass, $M = 1.3 \times 10^7\ M_\odot$ (Wang & Lu 2001), in contradiction to our conclusion based on the detection of the soft X-ray lines.

We are grateful to Suzy Collin for discussion regarding spectral models of the warm absorber computed by TITAN. We thank Liz Galle for help in processing the archival data and Antonella Fruscione and Fabrizio Nicastro for discussion. This work was supported in part by grant 2P03D00322 of the Polish State Committee for Scientific Research and by Jumelage/CNRS No. 16 "Astronomie France/Pologne." A. S. acknowledges support through NASA contract NAS8-39073 (CXC).

REFERENCES

Ballantyne, D. R., Ross, R. R., & Fabian, A. C. 2001, MNRAS, 327, 10
———. 2002, MNRAS, 336, 867
Boller, T., Brandt, W. N., & Fink, H. 1996, A&A, 305, 53
Boller, Th., Tanaka, Y., Fabian, A. C., Brandt, W. N., Gallo, L., Anabuki, N., Haba, Y., & Vaughan, S. 2003, MNRAS, 343, L89
Collin, S., Coupé, S., Dumont, A.-M., Petrucci, P.-O., & Różańska, A. 2003, A&A, 400, 437
Collin-Souffrin, S., Czerny, B., Dumont, A.-M., & Życki, P. T. 1996, A&A, 314, 393
Collinge, M. J., et al. 2001, ApJ, 557, 2
Comastri, A., et al. 1998, A&A, 333, 31
Czerny, B., & Dumont, A.-M. 1998, A&A, 338, 386
Czerny, B., & Elvis, M. 1987, ApJ, 321, 305
Czerny, B., & Życki, P. T. 1994, ApJ, 431, L5
Dickey, J. M., & Lockman, F. J. 1990, ARA&A, 28, 215
Done, C., Mulchaey, J. S., Mushotzky, R. F., & Arnaud, K. A. 1992, ApJ, 395, 275
Dumont, A.-M., Abrassart, A., & Collin, S. 2000, A&A, 357, 823
Kaastra, J. S., Steenbrugge, K. C., Raassen, A. J. J., van der Meer, R. L. J., Brinkman, A. C., Liedahl, D. A., Behar, E., & de Rosa, A. 2002, A&A, 386, 427
Kallman, T., & Bautista, M. 2001, ApJS, 133, 221
Kaspi, S., et al. 2000, ApJ, 533, 631
———. 2002, ApJ, 574, 643
Kawaguchi, T. 2003, ApJ, 593, 69
Kinkhabwala, A., et al. 2002, ApJ, 575, 732
Krolik, J. H. 2002, in X-Ray Spectroscopy of AGN with *Chandra* and *XMM-Newton*, ed. Th. Boller, S. Komossa, S. Kahn, & H. Kunieda (MPE Rep. 279; Garching: MPE), 131
Krolik, J. H., McKee, C. F., & Tarter, C. B. 1981, ApJ, 249, 422
Kurpiewski, A., Kuraszkiewicz, J., & Czerny, B. 1997, MNRAS, 285, 725
Leighly, K. M., Zdziarski, A. A., Kawaguchi, T., & Matsumoto, C. 2002, in X-Ray Spectroscopy of AGN with *Chandra* and *XMM-Newton*, ed. Th. Boller, S. Komossa, S. Kahn, & H. Kunieda (MPE Rep. 279; Garching: MPE), 259
Mason, K. O., et al. 2003, ApJ, 582, 95
Nayakshin, S., Kazanas, D., & Kallman, T. R. 2000, ApJ, 537, 833
Osterbrock, D. E., & Pogge, R. W. 1985, ApJ, 297, 166
Puchnarewicz, E. M., Mason, K. O., Siemiginowska, A., Fruscione, A., Comastri, A., Fiore, F., & Cagoni, I. 2001, ApJ, 550, 644
Romano, P., Turner, T. J., Mathur, S., & George, I. M. 2002, ApJ, 564, 162
Różańska, A., Czerny, B., Dumont, A.-M., Collin, S., & Siemiginowska, A. 2003, in ASP Conf. Ser. 290, Active Galactic Nuclei: From Central Engine to Host Galaxy, ed. S. Collin, F. Combes, & I. Shlosman (San Francisco: ASP), 249
Różańska, A., Czerny, B., Życki, P. T., & Pojmanski, G. 1999, MNRAS, 305, 481
Różańska, A., Dumont, A.-M., Czerny, B., & Collin, S. 2002, MNRAS, 332, 799
Stark, A. A., Gammie, C. F., Wilson, R. W., Bally, J., Linke, R. A., Heiles, C., & Hurwitz, M. 1992, ApJS, 79, 77
Sunyaev, R. A., & Titarchuk, L. G. 1980, A&A, 86, 121
Turner, T. J., George, I. M., & Nandra, K. 1998, ApJ, 508, 648
Turner, T. J., et al. 2001, ApJ, 548, L13
———. 2002, ApJ, 568, 120
Wang, T., & Lu, Y. 2001, A&A, 377, 52
Wisotzki, L., Dreizler, S., Engels, D., Fink, H.-H., & Heber, U. 1995, A&A, 297, L55
Yaqoob, T., McKernan, B., Kraemer, S. B., Crenshaw, D. M., Gabel, J. R., George, I. M., & Turner, T. J. 2003, ApJ, 582, 105